Molecular Therapy
Original Article

Deficiency of galactosyl-ceramidase in adult oligodendrocytes worsens disease severity during chronic experimental allergic encephalomyelitis

Natalia Saldivia,[1,3] Gregory Heller,[1,3] Diego Zelada,[1,3] Jason Whitehair,[1] Nikhil Venkat,[1] Ashna Konjeti,[1] Reina Savitzky,[1] Shayla Samano,[1] Daniel Simchuk,[2] Richard van Breemen,[2] Maria I. Givogri,[1] and Ernesto R. Bongarzone[1]

[1]Department of Anatomy and Cell Biology, College of Medicine, University of Illinois at Chicago, Chicago, IL, USA; [2]Linus Pauling Institute, Oregon State University, Corvallis, OR 97331, USA

Galactosyl-ceramidase (GALC) is a ubiquitous lysosomal enzyme crucial for the correct myelination of the mammalian nervous system during early postnatal development. However, the physiological consequence of GALC deficiency in the adult brain remains unknown. In this study, we found that mice with conditional ablation of GALC activity in post-myelinating oligodendrocytes were lethally sensitized when challenged with chronic experimental allergic encephalomyelitis (EAE), in contrast with the non-lethal dysmyelination observed in *Galc*-ablated mice without the EAE challenge. Mechanistically, we found strong inflammatory demyelination without remyelination and an impaired fusion of lysosomes and autophagosomes with accumulation of myelin debris after a transcription factor EB-dependent increase in the lysosomal autophagosome flux. These results indicate that the physiological impact of GALC deficiency is highly influenced by the cell context (oligodendroglial vs. global expression), the presence of inflammation, and the developmental time when it happens (pre-myelination vs. post-myelination). We conclude that *Galc* expression in adult oligodendrocytes is crucial for the maintenance of adult central myelin and to decrease vulnerability to additional demyelinating insults.

INTRODUCTION

Control of lipid homeostasis is essential for myelin stability and function in mammals.[1–11] Deficient activities of enzymes involved in the metabolism of cholesterol, plasmalogens, and glycosyl-sphingolipids alter the stoichiometric balance of lipids in the myelin membrane, increasing the vulnerability to demyelination and secondary damage to axons. Although galactosyl-ceramidase (GALC) is a ubiquitous acid lysosomal hydrolase, its expression in myelin-forming cells (i.e., oligodendrocytes and Schwann cells) is essential for the catabolism of galactosyl-ceramides and, in particular, galactosyl-sphingosine (psychosine).[12] A global deficiency of GALC and the consequent toxic accumulation of psychosine is the metabolic pathophysiological basis of Krabbe disease (KD) (also known as globoid cell leukodystrophy [GLD]), an inherited autosomal recessive leukodystrophy.[13,14] KD patients are largely infants and young adolescents, with a smaller fraction of patients presenting with milder clinical symptoms in late adolescence or adulthood.[14] Most of the pathogenetic mechanisms of demyelination, inflammatory gliosis, and neuronal dysfunction are triggered through the abnormal accumulation of psychosine in membrane lipid rafts early in life.[15]

Our laboratory and others have shown that perinatal reconstitution of GALC activity, mainly by gene therapy with adeno-associated viral vectors (AAVs), has a positive impact in protracting disease in both twitcher (Twi) mice and GLD dogs, preclinical KD animal models.[16–19] AAV therapy also led to near complete normalization of neurological readouts, motor skills, and neuropathology in the Twi mouse[18] and the GLD dog.[19] Despite this significant improvement, we and others have identified late-onset lesions in brain white matter of treated Twi mice, damage that was not present in treated Twi mice at younger ages.[20,21] These aging-related lesions correlated with local loss of GALC activity secondary to loss of the therapeutic AAV and the reoccurrence of psychosine-mediated disease.[21] These observations and additional studies showing deficient myelin responses to induced chemical demyelination in young adult haplo-insufficient Twi mice[22] underline the importance of preserving a functional GALC metabolism for myelin homeostasis throughout life.

Received 14 December 2023; accepted 24 June 2024;
https://doi.org/10.1016/j.ymthe.2024.06.035.

[3]These authors contributed equally

Correspondence: Natalia Saldivia, Department of Anatomy and Cell Biology, College of Medicine, University of Illinois at Chicago, 808 S. Wood St M/C 512, Chicago, IL, USA.
E-mail: nsaldivi@uic.edu
Correspondence: Ernesto R. Bongarzone, Department of Anatomy and Cell Biology, College of Medicine, University of Illinois at Chicago, 808 S. Wood St M/C 512, Chicago, IL, USA.
E-mail: ebongarz@uic.edu

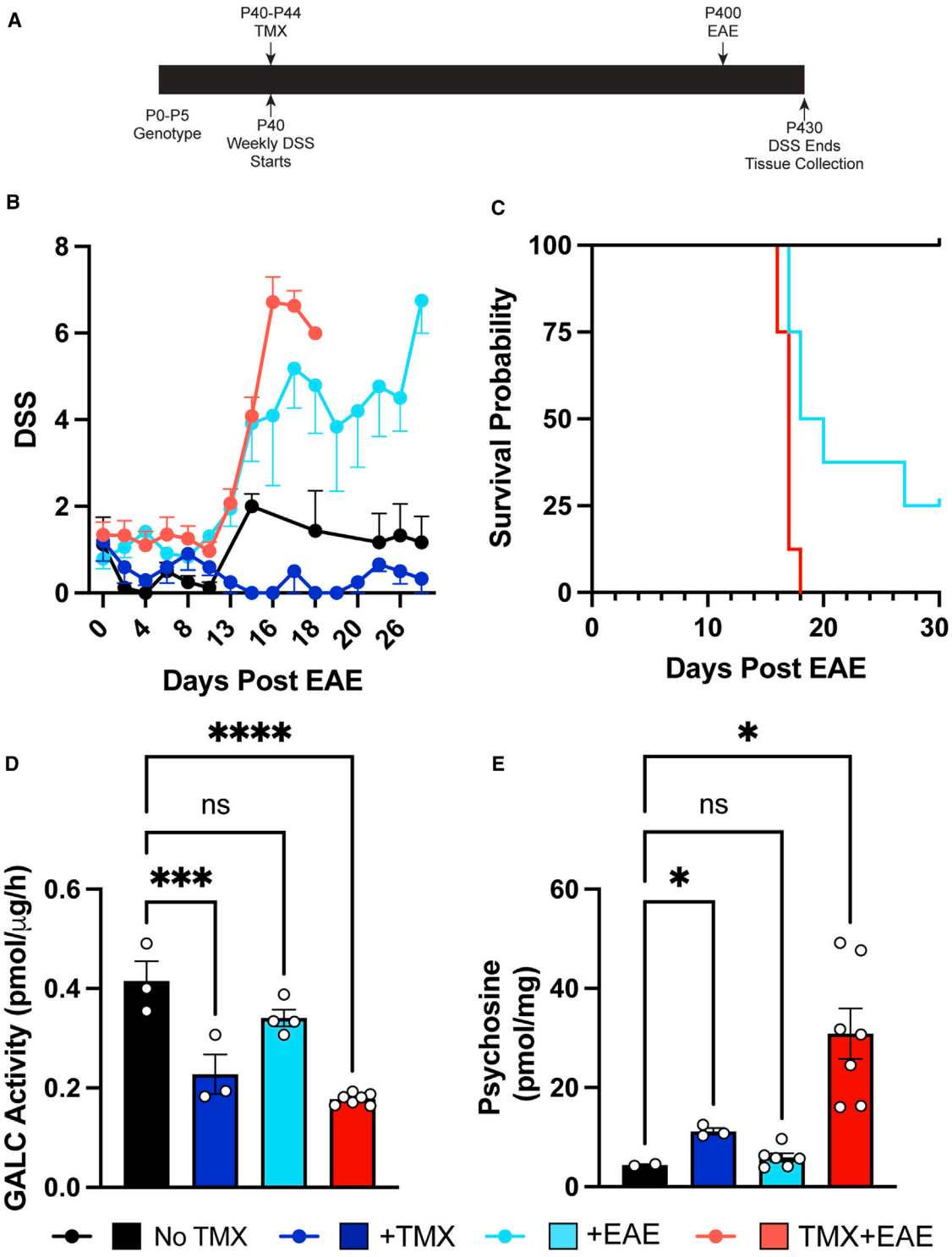

Figure 1. Ablation of *Galc* expression in adult oligodendrocytes transformed the chronic presentation of MOG-EAE into a fulminant acute disease

(A) Experimental paradigm to assess the impact of *Galc* deletion in mature oligodendrocytes on the clinical manifestation of EAE in *PLP-CRE*^{ERT}*-Galc*$^{f/f}$ mice. (B) DSS was measured in TMX+EAE mice during the 30 days after EAE induction or until mice reached humane end point criteria. Control groups included +EAE (EAE+*PLP-*

(legend continued on next page)

Most of our current knowledge on GALC function comes from studies done in early postnatal life in wild-type and *Galc* mutant animals and cell cultures.[23–29] However, there are no formal studies examining the role of GALC after myelination is completed in the mammalian brain. The lack of models to conditionally and cell specifically ablate *Galc* was a limitation for these types of studies. The recent generation of a lox-P-inducible *Galc* knockout transgenic line[30] enabled us to perform such studies. Considering that oligodendrocytes must also maintain healthy myelin throughout life, we hypothesized that the loss of function of GALC after myelination is complete negatively impacts on the long-term stability of myelin and its vulnerability to demyelination.

In this work, we crossed loxP-*Galc* transgenic mice[31] with *PLP-CRE-*^{ERT} mice[32] and generated conditional *Galc* ablated mice with deficiency restricted to post-mitotic PLP^{+} oligodendrocytes between postnatal days (P) P40 and P44. By this genetic approach, we studied the functional role of the GALC enzyme in adult myelin stability and vulnerability to disease when challenged to chronic experimental allergic encephalomyelitis (EAE).[33,34]

RESULTS

Conditional loss of function of GALC in mature oligodendrocytes sensitized mice to EAE with fulminant demyelination

In this study, we evaluated the extent to which the adult loss-of-function of the *Galc* gene in post-mitotic oligodendrocytes is a worsening factor for the progression and intensity of EAE, the most used experimental model for multiple sclerosis (MS). For this, we used a conditionally regulated floxed line to ablate *Galc* expression only in PLP^{+} oligodendrocytes.[32] Tamoxifen (TMX) recombination was initiated at P40 when the mouse brain is mostly myelinated,[35] while EAE was induced by immunization with myelin oligodendrocyte glycoprotein (MOG) at P400[33] (Figure 1A).

Experimental groups were assessed using our Disease Severity Scoring (DSS) system for 30 days after immunization.[18] Notably, all mice with ablation of *Galc* in oligodendrocytes exhibited increased DSS scores from 13 days after EAE and rapidly deteriorated (Figure 1B) to the point that by human end point Institutional Animal Care and Use Committee criteria, all double challenged mice had to be euthanized by 18 days after immunization (Figure 1C). In contrast, EAE in mice with normal *Galc* expression underwent a stereotypical EAE disease (Figure 1B) with approximately one-half of the EAE^{+}, non-TMX mice reaching humane end point by 21 days after EAE and many surviving throughout the 30-day experiment (Figure 1C). The control groups, +TMX, and non-TMX displayed minor and insignificant DSS signs (Figure 1B), variations attributed to aging (e.g., fluctuations in body weight in aged mice are noticeable) and lived throughout the 30-day experiment without any impairment or death (Figure 1C). *In vitro* and *in vivo* quality control of CRE-recombination confirmed correct ablation of *Galc* only in oligodendrocytes with expected decreases in enzyme activity and psychosine increases (Figures S1 and S2).

GALC activity was evaluated in brain lysates (Figure 1D) and, as expected, +TMX mice regardless of EAE, exhibited significantly reduced GALC activity (Figure 1D). The roughly 50% decrease in GALC activity (Figure 1D) and the lack of significant changes in ACD activity[36] (Figure S3) converged in significant increases in psychosine levels in TMX+EAE and +TMX brain lysates (Figure 1E). The higher levels of psychosine detected in TMX+-EAE mice respect +TMX mice (Figure 1E) correlated with a robust deterioration of microglial activity in the double challenged TMX+EAE mice (see below). Together, these data highlight that GALC deficiency in mature oligodendrocytes elevates the susceptibility to additional demyelinating stressors such as EAE and involves a toxic accumulation of psychosine. Furthermore, ablation of *Galc* in adult oligodendrocytes is sufficient to change EAE presentation from a chronic condition to an acute fulminant disease.

Loss of function of GALC in mature oligodendrocytes enhanced demyelination, gliosis, and inflammation in EAE mice

To examine the extent of demyelination, gliosis, and inflammation, brain tissue from terminal animals was immunostained for the expression of myelin proteolipids (PLPs), which enabled us to differentiate areas with intact myelin from those lacking myelin,[37] GFAP, CD68, and Iba-1. In demyelinated areas, significant levels of PLP^{+} myelin debris were observed (Figures 2I, S4G, S5G, and S6G). Marked levels of demyelination with an abundance of myelin debris were observed in the cerebellar deep white matter (Figure 2A), medulla oblongata (Figure S4), and hippocampus (Figure S5), and less evident in cortical areas (Figure S6) of TMX+EAE mice. Mild regional dysmyelination in the same aforementioned areas (Figures S4C–S4F and S5C–S5F) was observed in +TMX mice. The cerebral cortex of +TMX mice showed apparently normal myelination (Figures S6C–S6F).

Demyelination was accompanied by a sharp increase in GFAP+ astrocytes and CD68+ and Iba-1 microglia in both TMX+EAE and +EAE mice groups. Astrogliosis in both groups was evidenced within the same regions but to a greater extent than in +TMX mice (Figures 2A, 2B, 2J, S4A, S4B, S4H, S5A, S5B, and S5H). Gliosis in cortical areas was not changed significantly (Figure S6). Similarly, our western blot analysis showed elevated levels of GFAP in all conditions compared with the control (Figures S7A and S7B). We also observed a significant increase in CD68^{+} cells in demyelinated areas

CRE^{ERT}*-Galc*$^{f/f}$), +TMX (TMX+*PLP-CRE*^{ERT}*-Galc*$^{f/f}$), and no-TMX (corn oil + mineral oil treated *PLP-CRE*^{ERT}*-Galc*$^{f/f}$ mice). (C) Lifespan probability analysis is shown in the Kaplan-Meier plot. *N* = 3 animals for No TMX and +TMX groups; *N* = 9 animals for +EAE and *N* = 12 for TMX+EAE conditions. (D and E) GALC activity and (E) psychosine levels were determined in total brain lysates. Graphs represent the mean ± SEM. ns: $p > 0,05$; $^{*}p < 0.05$; $^{***}p < 0.001$; $^{****}p < 0.0001$ (one-way ANOVA, followed by Tukey *post hoc* test). *N* = 3–9 mice/group. ns, not significant.

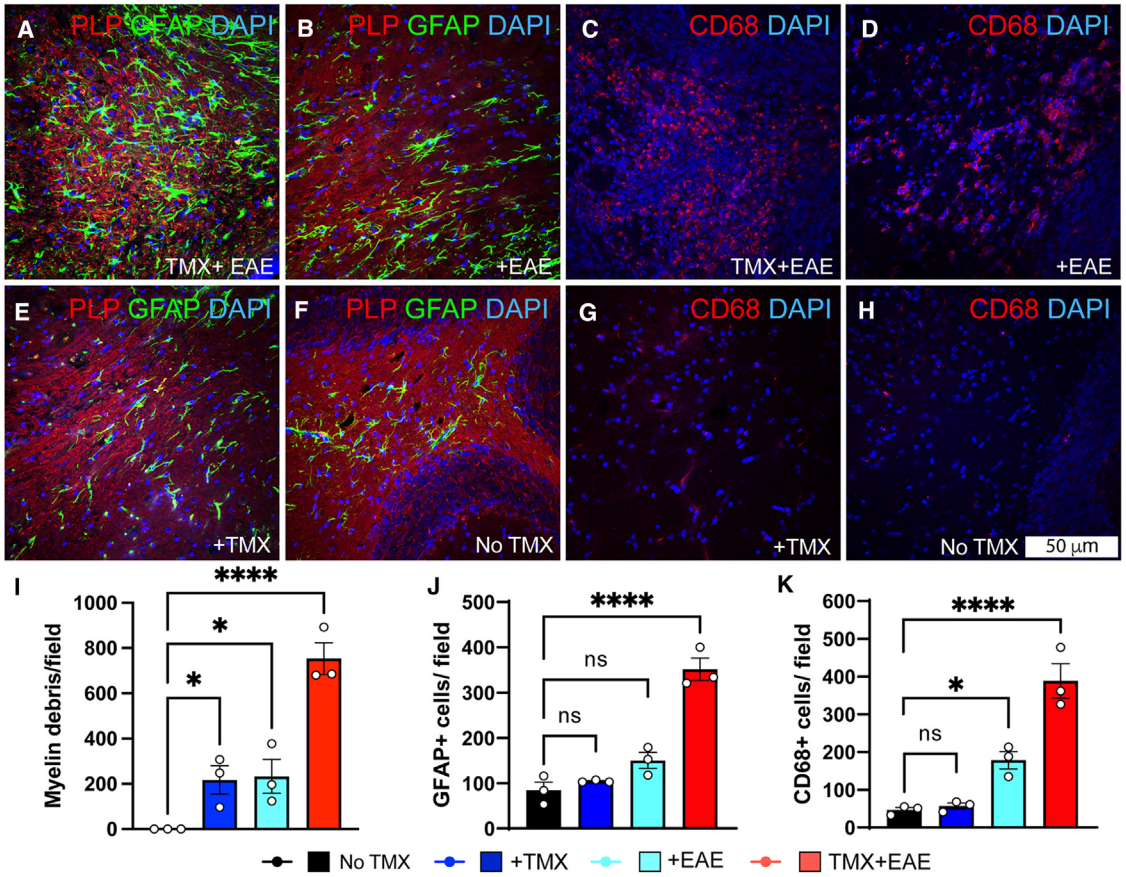

Figure 2. Ablation of *Galc* expression in adult oligodendrocytes increased demyelination and gliosis after EAE induction

(A–H) The effects of *Galc* ablation in oligodendrocytes upon EAE induction on demyelination and gliosis was evaluated in P430 brain sections by immunohistochemistry using antibodies against the myelin PLPs (red) and GFAP (green) (A, B, E, and F), or CD68 (red) (C, D, G, and H). Nuclei were counter stained with DAPI (blue). Confocal microscopy images of deep cerebellar white matter are shown. (I–K) Myelin debris per field was quantified in the deep cerebellar white matter for each condition. The number of GFAP$^+$ (J) and CD68$^+$ cells (K) per field was quantified. Graphs represent the mean ± SEM for each condition. $p > 0.05$; $^*p < 0.05$; $^{****}p < 0.0001$; ns, not significant ($p > 0.05$) (one-way ANOVA, followed by Tukey *post hoc* test). $N = 3$ mice/group. Data points represent the average value for each quantification per mouse.

at the deep cerebellar white matter of TMX+EAE and +EAE, but not of the +TMX or control mice (Figures 2C, 2D, 2G, 2H, and 2K). Western blotting confirmed a significant increase in the levels of CD68 immunodetectable bands in both EAE experimental groups (Figure S7A and S7C). Iba-1-positive cells were abundant in both the TMX+EAE and +EAE groups (Figure S8), with significant increases of Iba-1 cells in the cerebellum (Figure S8M), hippocampus (Figure S8N), and corpus callosum (Figure S8O). Iba-1 cells were moderate but significantly increased in the +TMX mice group (Figures S8M and S8N). In general, demyelinated fibers were always surrounded by filopodia from astrocytes and Iba-1+ microglia, which was more evident in TMX+EAE mice (Figure S9, arrows).

Importantly, active caspase-3 levels were significantly increased after induction of EAE in +TMX mice (Figures S7A and S7D), suggesting that the combination of *Galc* ablation in oligodendrocytes and EAE led to a substantial apoptotic cell death. Further typification confirmed that, in all three conditions, the cells undergoing apoptosis were chiefly oligodendrocytes and microglia and to a much lesser extent neurons, astrocytes, and OPCs (Figures S10–S15).

Loss of function of GALC in mature oligodendrocytes impaired remyelination in EAE mice

Ablation of *Galc* in adult oligodendrocytes negatively impacted the levels of platelet-derived growth factor receptor-α (PDGFRα), Olig2, and Sox10 in demyelinated areas of EAE mice (Figures 3F–3I). We examined the remyelination capacity in the +TMX brain by counting dividing OPCs in the cervical spinal cord, a region that also shows clear signs of demyelination. OPCs were labeled with antibodies against NG2 and Sox10, which are markers for OPCs and are involved in their differentiation into myelinating oligodendrocytes. Dividing cells were identified using an antibody to PCNA. Even though some NG2+ OPCs were observed (Figure 3A), proliferating (PCNA+) Sox10+ OPCs were barely found in the spinal cord white matter in TMX+EAE mice (Figures 3C and 3E). Mice subjected to EAE with normal GALC levels also exhibited significantly fewer

OPCs when compared with the control groups, but a fraction of OPCs in these animals were undergoing cell division (Figures 3D and 3E), indicating that remyelination is occurring to some extent. However, transmission electron microscopy (TEM) analysis (Figures 3J–3N) confirmed that, although there were more axons showing signs of demyelination in TMX+EAE mice, fewer axons were in the process of remyelination (Figures 3J, asterisk, 3N). In contrast, the +EAE group exhibited significant levels of both demyelinated axons and remyelination (Figures 3K and 3N). In contrast, while there were some demyelinated axons in +TMX cords, the percentage of these axons did not differ significantly from the control group (Figures 3L and 3N). +TMX mice also showed significantly lower numbers of NG2+ and Sox10+ OPCs, yet they showed an increase in dividing OPCs ($Sox10^+$/$PCNA^+$ cells) (Figures S16A–S16E and 3E), suggesting proliferation to support a weak remyelination (Figures 3L and 3N).

Importantly, when we evaluated the long-term impact of *Galc* deletion in adult PLP+ oligodendrocytes, +TMX mice showed mild motor deficits, with the greatest relative deficits in the ledge balance test as compared with control mice (Figure S17D). No significant differences were observed in weight, grip strength, and locomotor activity (Figures S17F–S17H). When evaluating the motor coordination of mice on an accelerating rotarod, +TMX mice performed significantly worse than the control mice at P240 (Figure S17E), aligning with the deficits observed in the ledge balance test. This did not significantly affect the survival of PLP-restricted *Galc*-deficient mice (Figure S17C). The control group mice showed minor, insignificant DSS signs (Figure S17B). These variations may be due to aging, as aged mice often experience noticeable fluctuations in body weight (Figure S17F). Of importance, although some reports have indicated that treatment with TMX may elicit some side effects,[38–40] wild-type control mice treated with TMX only did not show any change in myelination, body weight, and motor skills (data not shown).

These data suggest a strong synergistic effect between the reduction of GALC activity in mature oligodendrocytes and EAE, turning in an acute, non-surviving, highly damaged, and poorly remyelinating demyelinating disease.

Loss of function of GALC did not promote globoid cell formation and impaired the lysosomal autophagosomal flux upon EAE induction

Globoid cells are one of the hallmarks of KD. In the Twi brain, multinucleated $CD68^+$ active globoid cells are abundant (Figure S18A, arrows), in sharp contrast to the stereotypical ramified single-nucleated CD68 resting microglia found in healthy brains (Figure S18B, arrow). While the ablation of *Galc* in adult oligodendrocytes in +TMX mice elicited a mild microglia activation (Figure 2K), all $CD68^+$ cells were single nucleated without any evidence of globoid cell formation (Figure S18C, arrow). Globoid cells were not observed in either +EAE (Figure S18D, arrow) or TMX+EAE (Figures S18E–S18I, arrow) mice. Notably, all three experimental conditions showed the presence of visible $CD68^+$ vacuoles in microglial cells (Figures S18G–S18I, arrowheads).

Being that CD68 protein also a type I membrane protein that shuffles between lysosomes and the plasma membrane,[41] the presence of enlarged $CD68^+$ vacuoles suggested of abnormalities within the lysosomal compartment. A common finding in lysosomal storage diseases such as KD is the deficit in the lysosome autophagosome flux (LAF).[42–44] LAF is tightly regulated and responds to cellular demands. For example, cellular stress, starvation, and removal of cell debris are potent stimuli that activate the transcription factor EB (TFEB)-coordinated lysosomal expression and regulation (CLEAR) axis[45,46] with the goal of recycling cellular components. To examine the contribution of changes in LAF in our disease model, we first focused on the two most stereotypical lysosomal-associated membrane proteins (LAMPs), LAMP1 and LAMP2. Immunodetection of these major lysosomal proteins showed an important increase in levels of immunodetectable LAMP1 in white matter tracts of either TMX+EAE (Figure 4A, insets), +TMX (Figure 4B, insets) or +EAE (Figure 4C, insets), compared with the basal levels in non-TMX mice (Figure 4D, insets). Remarkably, LAMP2 expression seemed to be markedly decreased in all three experimental conditions, falling below the levels observed in non-TMX mice (Figures 4A–4D). Western blotting (Figure 4N) confirmed an increase of LAMP1 (Figure 4Q) and approximately a 60% decrease of LAMP2 in the +TMX and +EAE brain (Figure 4R) with respect to control levels in the non-TMX brain. Interestingly, LAMP2 levels showed further reduction (approximately 75%) in the TMX+EAE brain (Figure 4R). Autophagic (p62, beclin1, and LC3I/II) markers were then studied to examine whether autophagy was also altered. Co-labeling with p62 and LAMP1 showed lack of co-localization of p62 and LAMP1 in all three experimental conditions suggesting an impaired fusion of lysosomes and autophagosomes (Figures 4E–4H, insets). In fact, we observed significant increases in the abundance of p62, particularly in the TMX+EAE brain (Figure 4E), which were confirmed by western blotting (Figure 4N) quantitative analysis (Figure 4T). This apparent increase in autophagosomes was further supported by western blotting analysis (Figure 4N) for LC3I/II (Figure 4S) and beclin1 (Figure 4U).

Lysosomal biogenesis is largely regulated through the nuclear activity of TFEB (Figure 4M). Nuclear TFEB activity depends on phosphorylation status at S211. Under normal conditions, activation of mTORC1 at the lysosomal membrane (via phosphorylation by active AKT-P-S473, Figure 4M) phosphorylates TFEB at S211, which is retained in the cytoplasm. Upon cellular stress, dephosphorylated (either by down-regulation of the AKT-mTORC1 axis or by the activity of PPP3-calcineurin) TFEB is translocated to the nucleus where it promotes the transcription of CLEAR genes. We evaluated phosphorylation levels of TFEB at S211 as well as AKT at S473 (Figure 4N). In consonance with the increase of LAMP1 expression, we found that phosphorylated TFEB was significantly decreased in +TMX and +EAE mice (approximately 60% and approximately 70%, respectively), but particularly in TMX+EAE mice (approximately 80%) (Figure 4P). Similarly, the upstream regulator of mTORC-1, phosphorylated AKT was also reduced (Figure 4O). Immunodetection of TFEB clearly showed that TFEB

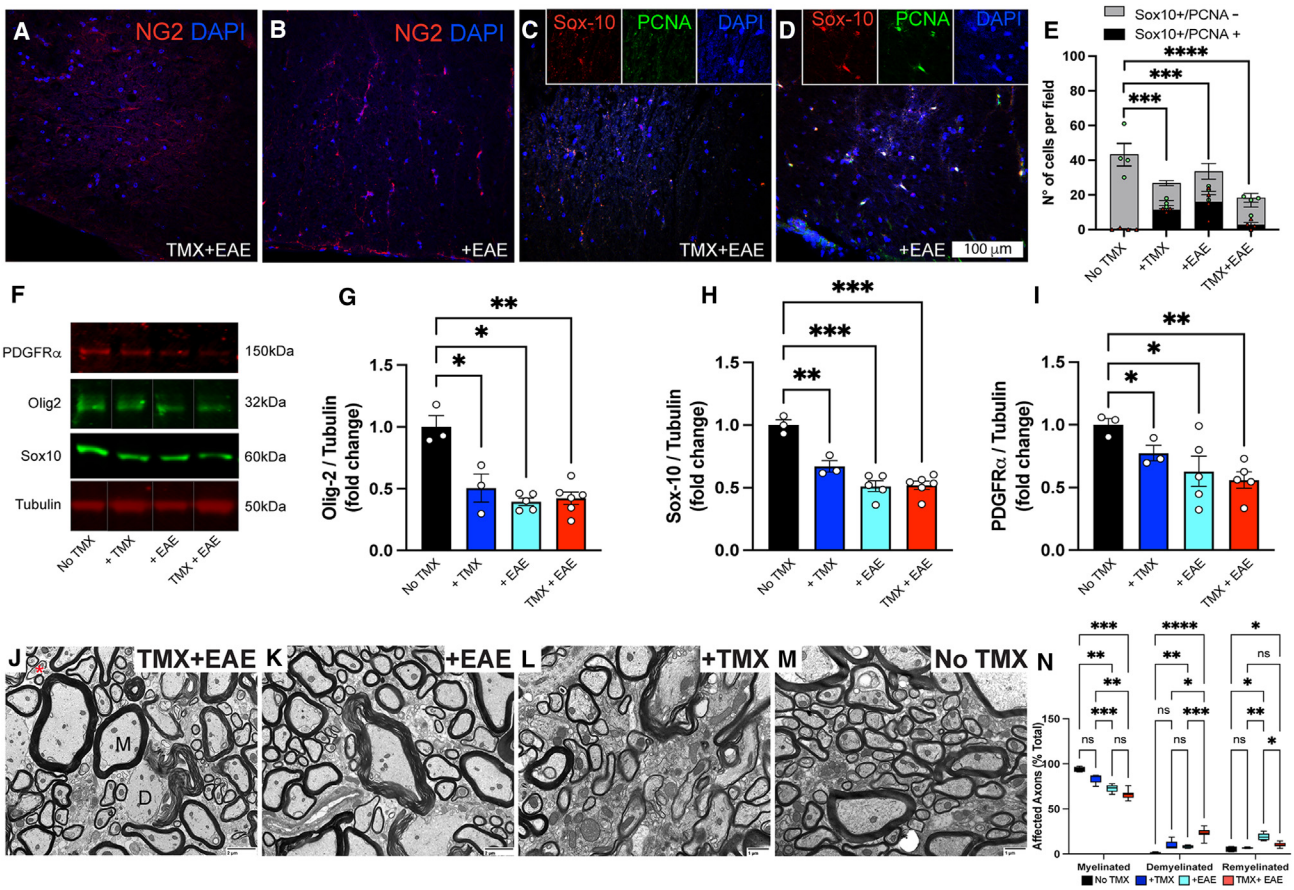

Figure 3. Impaired remyelination in mice with ablated *Galc* expression in adult oligodendrocytes during EAE

(A–D) The impact of EAE in mice subjected to *Galc* ablation in oligodendrocytes on OPC response was evaluated in cross-sections of P430 cervical spinal cords by immunohistochemistry followed by confocal microscopy. Analyses were performed using an antibody against NG2 (red) (A and B), or Sox-10 (red) and PCNA (green) (C and D). Nuclei were counter stained with DAPI (blue) to reveal the total number of cells per field. (E) Graphs represent the total number of Sox10$^+$ cells in each condition (Sox10$^+$/PCNA$^-$, gray bars), as well as the number of Sox10$^+$ cells that were also PCNA$^+$ (Sox10$^+$/PCNA$^+$, black bars). (F–I) P430 brain lysates were subjected to western blot analysis using antibodies against PDGFRα, Olig2 and Sox10. Gray rectangles depict different bands located within the same gel. The ratio of band intensity against tubulin was quantified for Olig2 (G), Sox10 (H) and PDGFrα (I) and normalized against control (No TMX) condition. Graphs represent the mean ± SEM. (J–M) The effect of *Galc* ablation in oligodendrocytes on remyelination was evaluated by TEM of cervical spinal cords ultra-thin sections obtained from the different experimental groups. (N) The percentage of myelinated, demyelinated and remyelinated axons were quantified and represented as the number of affected axons for each condition. In image (J): M, myelinated axon; D, demyelinated axon; red asterisk, remyelinated axon. Graphs represent the mean ± SEM. *$p < 0.05$; **$p < 0.01$; ***$p < 0.001$; ****$p < 0.0001$ (Student t test). $N = 3$ animals were employed for No TMX and +TMX groups, whereas $N = 6$ animals were used for +EAE and TMX+EAE conditions.

translocated to the nucleus of cells of TMX+EAE (Figure 4I), +EAE (Figure 4K), and +TMX (Figure 4J) spinal cords, in comparison with the mostly cytoplasmic localization in the control non-TMX (Figure 4L) cord.

Collectively, these findings reveal that GALC deficiency in oligodendrocytes, EAE induction, or a combination of both insults leads to the activation of TFEB. TFEB activation in turn promotes and up-regulates autophagy-lysosomal biogenesis. However, fusion of lysosomes and autophagosomes seemed to be compromised, which in mice with *Galc* ablated and EAE may lead to a critical bottleneck in the removal of myelin debris and reinforcement of inflammation. Notably, TFEB has also been indicated to repress the differentiation of OPCs in myelinating oligodendrocytes, which may underline the poor remyelination measured in our study.[47]

DISCUSSION

GALC is a lysosomal enzyme crucial for the early postnatal metabolism of myelin. This notion has been demonstrated using *Galc*-deficient TWI mice, GLD dogs, and autopsy material from KD patients.[18,19,31,48–52] However, the extent to which GALC has similar physiological roles in the adult brain remains unexplored. In addition to its well-established pathogenetic role in KD, *GALC* has recently been identified in genome-wide association studies and biochemical analyses as a risk gene in other adult-onset neurodegenerative conditions, including Parkinson disease[53,54] and MS.[55] A case report[56] and

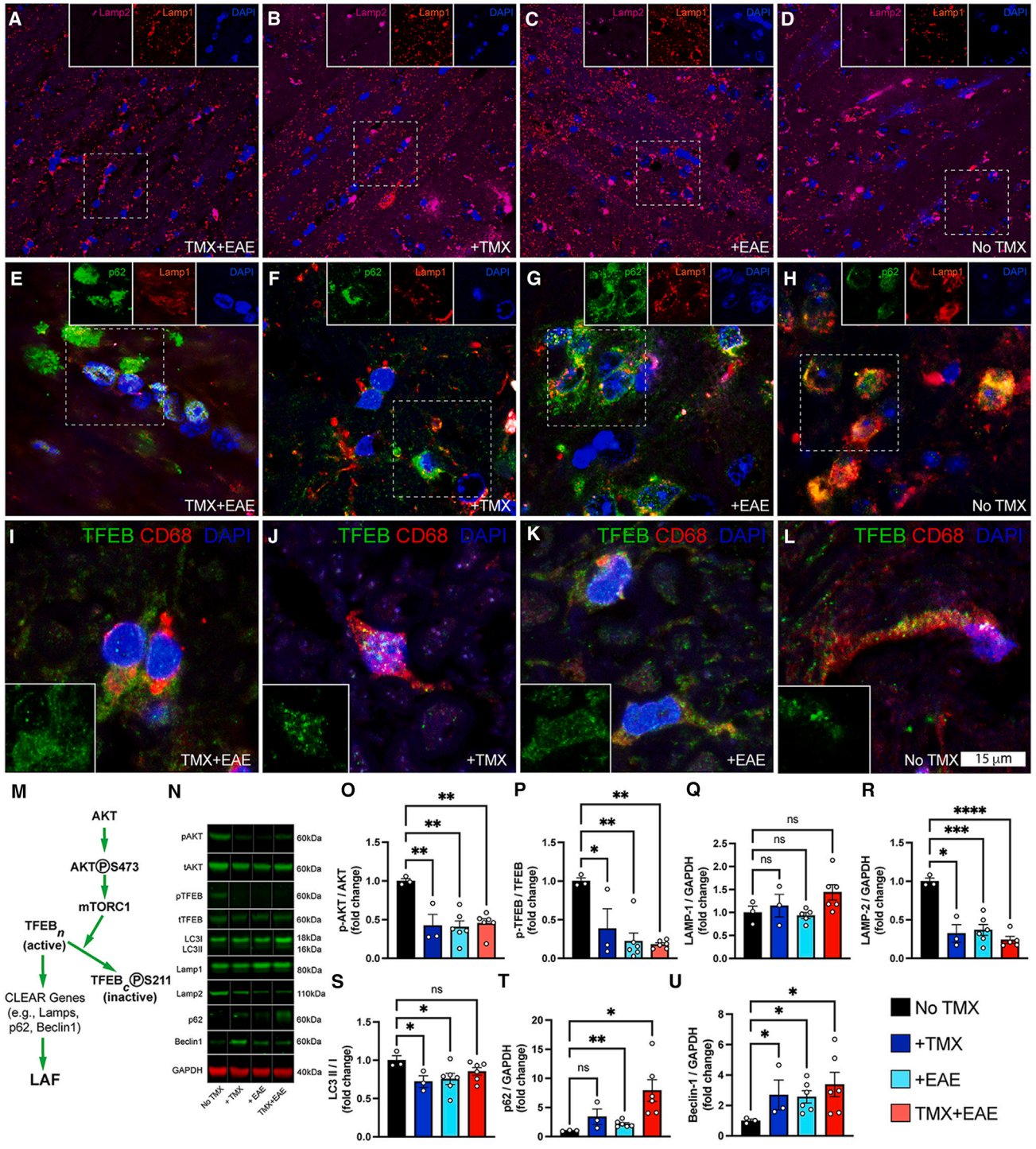

Figure 4. Increased TFEB-mediated CLEAR response with impaired lysosomal autophagosomal flux

(A–H) Immunohistochemistry analysis of brain sections from TMX + EAE, as well as control groups (EAE + No TMX+; +TMX and No TMX) was performed using antibodies against LAMP-1 (red) and LAMP-2 (magenta) (A–D), or p62 (green) and LAMP1 (red) (E–H). (I–L) TFEB localization was evaluated by immunohistochemistry analysis of cervical spinal cord cross-sections using antibodies anti-TFEB (green) and CD68 (red). Nuclei were stained with DAPI (blue). (M) Diagram representing the molecular pathway of AKT-mTORC1-mediated regulation of TFEB activity, a master promoter of lysosome biogenesis. Briefly, phosphorylated (active) AKT at serine 473 (S473) leads to mTORC1 phosphorylation and activation, which leads to downstream phosphorylation of TFEB at Ser211 (S211). S211-phosphorylated TFEB is no longer able to translocate to the

(legend continued on next page)

several personal communications of KD pedigrees with adult family members developing MS and down-regulation of *GALC* expression in some MS patients[57] reinforce the possibility that reductions of GALC activity increase the risk to develop MS.

To start examining this hypothesis, we generated an MOG-induced EAE model of MS[33,34] using mice with conditional ablation of *Galc* expression[30] in post-mitotic oligodendrocytes.[32] Induction of EAE in adult TMX-treated *PLP-CRE^{ERT}-Galc$^{f/f}$* mice led to a fulminant and deadly acute form of EAE with 100% obligate euthanasia by 18 days after immunization in contrast with control EAE mice with more than approximately 50% of mice fully recovering from EAE. This notable and distinct presentation of the disease in the doubly challenged TMX+EAE mice involved a strong demyelination, significant accumulation of myelin debris throughout the brain and spinal cord, and poor remyelination. TMX side effects including changes in bone, temperature, movement, and contradictory effects on myelination have been reported.[38–40] In our experimental conditions, control mice treated only with TMX (data not shown) did not show any myelination and behavioral changes that could significantly have accounted for the above reported differences in survival and disease severity in TMX-treated, EAE-treated, and doubly challenged TMX+EAE animals.

As expected, demyelination in the double-challenged model was accompanied by significant levels of cell death among mature oligodendrocytes and approximately a 2.5-fold increase in psychosine respect levels in the non-EAE *Galc*-ablated controls. We did not find significant changes in ACD activity in the double-challenged model, suggesting that the increased levels of psychosine correlated better with the noted abundance of myelin debris than from *de novo* synthesis.[36] Despite the decrease in GALC, psychosine accumulation was overall modest in all experimental conditions. This could be caused by some level of cross-correction of ablated oligodendrocytes by GALC produced in neighboring cells.[58] How much GALC was cross-corrected by individual cells remains uncertain. Because ablation of *Galc* occurred only in mature PLP+ oligodendrocytes, neighboring neurons, astrocytes, and microglia may all serve as endogenous sources of secretable GALC, which if reaching *Galc*-ablated oligodendrocytes may decrease the magnitude of the deficiency in these cells. Differential cell sensitivities to take up lysosomal enzymes have been suggested from work done with aryl-sulfatase A,[59] and while direct extrapolations to GALC cannot be done, we could speculate on several factors affecting the overall efficiency of GALC cross-correction in the brain, including level of enzyme production and secretion by individual cells, degree of phosphorylation of mannose-6 residues in the enzyme, and expression of active mannose-6-phosphate receptors on the surface of oligodendrocytes.[59] Planned studies using the new lysosomal membrane-tethered GALC (*Galc-LAMP1*) transgenic line, where cross-correction is blocked,[60] will help to determine how much cross-correction contributes to the final metabolic effect.[30] Low levels of psychosine may also reflect an overall decrease in psychosine synthesis by the ACD anabolic pathway in the adult brain,[36] especially because in our model CRE-ablation of *Galc* occurred between P40 and P44, after central myelination was largely completed. In addition, our model involved CRE-mediated ablation after myelination completion (P40–P44), with analysis conducted on aged mice (P400). Over time, oligodendrocytes lacking GALC may have been gradually replaced by newly formed oligodendrocytes derived from resident quiescent OPCs, with normal unaffected expression of *Galc*. However, this long-term cell replacement did not fully mitigate the early recombination effects, leading to increased psychosine levels and myelin damage in adult ablated animals. Future experiments employing a combination of PLP and PDGFRα promoters for CRE^{ERT} recombination could further elucidate this aspect.

Our results showed that TMX+EAE in *PLP-CRE^{ERT}-Galc$^{f/f}$* mice had significantly decreased levels of PDGFRα, Sox10, and Olig2, key for the successful recruitment and migration of OPCs to engage in productive remyelination. Decreased expression of these genes may have contributed a lack of productive remyelination in mice facing the double challenge. It is well established that successful remyelination also requires an intact phagocytic capacity of microglial cells to remove myelin debris to enable the recruitment and engagement of OPCs.[61–63] We found that TMX+EAE-treated *PLP-CRE^{ERT}-Galc$^{f/f}$* mice indeed developed a robust microglial and macrophage presence with high numbers of CD68^{+} and Iba1^{+} cells associated with demyelinating areas. However, despite this robust inflammatory response, myelin debris were poorly removed (marked by the abundance of PLP^{+} myelin remnants in major white matter areas). This underlines that, over time, the capacity of microglia and infiltrating macrophages to phagocyte and remove myelin debris waned in the doubly challenged mice. We suspect that this is non-cell autonomous maladaptive innate response of microglial cells to an increased toxicity from psychosine-enriched myelin membranes.[64] Multiple studies have shown that microglial cells can be non-cell autonomously impaired. For example, poor microglia function was observed in models of myelin damage,[61,65] or when pro-inflammatory signaling fails,[66] and even when exposed to toxic Aβ in Alzheimer disease.[67,68] Another study where Twi heterozygous mice were exposed to non-inflammatory cuprizone

nucleus, and thus becomes inactive. (N–U) Brain lysates were subjected to western blot analyses to determine the levels of phosphorylation of the AKT-mTORC1-TFEB signaling pathway, along with lysosomal and autophagy proteins as a readout of LAF. Phospho-AKT (AKT-P-S473), phospho-TFEB (TFEB-P-S211), total AKT (tAKT) and TFEB (tTFEB), LC3 I/II, p62, beclin-1, LAMP-1 and LAMP-2 antibodies were used for each condition. GAPDH antibody was employed as loading control. Gray rectangles depict different bands located within the same gel. Band intensities were quantified for each condition, normalized against GAPDH levels, and fold changes normalized to the control (No TMX) group calculated for phospho-AKT/AKT (O), phospho-TFEB/TFEB (P), LAMP-1 (Q), LAMP-2 (R), LC3 II/I (S), p62 (T), and Beclin-1 (U). Graphs represent the mean ± SEM. $^{*}p < 0.05$; $^{**}p < 0.01$; $^{***}p < 0.001$; $p < 0.0001$ (one-way ANOVA, followed by Tukey *post hoc* test). $N = 3$ animals were employed for no TMX and +TMX groups, whereas $N = 6$ animals were used for +EAE and TMX+EAE conditions.

demyelination[22] also showed deficiencies in remyelination and microglia responses, although without a lethality as seen in our TMX+ EAE model. Notably, our study differs in that GALC deficiency was only done in mature oligodendrocytes but not in microglia, thus, underlining a non-cell autonomous defect impairing the innate capacity of microglia to remove damaged myelin when challenged with EAE. The lack of lethality and the modest demyelination observed in +TMX mice underlines that in the absence of additional stressors affecting myelin integrity (i.e., EAE), GALC deficiency in adult oligodendrocytes is per se insufficient to compromise survival or trigger a severe neurological phenotype. Future experiments will test whether *Galc* ablation in mature oligodendrocytes as well as in microglia synergize to make mice more sensitive to EAE. The combination of multiple factors may play important pathognomonic roles in neurodegeneration, disease presentation, and disability observed in adult-onset myelin disorders such as MS.[69–71] In this sense, our results underline that carrying mutations in the *Galc* gene in the presence of additional environmental and/or genetic factors may render *GALC* carriers more vulnerable.

In addition to the maladaptive response of microglial cells, EAE and *Galc* deficiency in oligodendrocytes seemed to target the regulation of the LAF pathway. This pathway is crucial when cells undergo stress conditions and need to recycle, remove, and degrade toxins, damaged organelles, and other cellular components. TFEB is a master transcription factor regulator of the CLEAR genes,[72] and therefore, has a prime role in modulating autophagy and lysosomal biogenesis. Our results showed severe changes in many readouts of LAF, with decreases in LAMP-2, and increases in p62 and beclin1, proteins involved in the biogenesis of lysosomes and their fusion with autophagosomes. Not surprisingly, we found increased activation (i.e., less phosphorylated TFEB at S211 and nuclear translocation) of TFEB associated with decreased activation of the AKT pathway in all three challenged conditions with respect to control levels, indicating that the recruitment of the pathway to aid in cellular clearance responded. However, the decreased levels of LAMP-2 and increased levels of p62 and beclin-1 suggest that the late steps of autophagosome and lysosome maturation are impaired, with significant accumulation of autophagosomes without obvious fusion to lysosomes. LAMP-2 knockout mice exhibit a massive accumulation of autophagic vacuoles,[73,74] which seems to be consequent to impaired autophagosome maturation.[73] Our results revealed a marked presence of vacuoles expressing the lysosomal protein CD68[41] in all experimental conditions. This accumulation may be related to the decreased levels of LAMP-2. Interestingly, autophagy is highly dysfunctional in the Twi brain,[42] with large cytoplasmatic aggregates of p62 and increases in beclin-1 levels,[42] changes that are also present in other neurodegenerative and lysosomal disorders, EAE, and MS.[75–80] Of relevance, inhibition of mTORC1, which is an intermediate regulator of TFEB, as well as a restoration of autophagy ameliorated neurological deficits in Twi mice.[42] This supports the idea that the proper assembly and function of autolysosomes is key for the degradation of toxic molecules, including psychosine, which is a known inhibitor of AKT activation.[81]

The up-regulation of active TFEB may have also contributed to reduce remyelination, as TFEB is a known suppressor of myelination.[47] Hence, the fulminant effects triggered by EAE in TMX-treated *PLP-CRE^{ERT}-Galc$^{f/f}$* mice may involve a multitude of contributing factors, including a dual role of TFEB. On one hand, TFEB activates the CLEAR response, and concomitantly, it induces the inhibition of remyelination by blocking the formation of myelinating oligodendrocytes.

In summary, our study contributes with insights on the interplay between genetic factors, such as GALC deficiency, and external triggers, such as EAE, in the context of demyelinating diseases. Although adult GALC deficiency alone in oligodendrocytes seems insufficient to generate a disease analogous to KD, enzyme deficits may be a risk factor to develop major demyelinating phenotypes such MS when combined with additional stressors. Therefore, further research is warranted to elucidate the susceptibility of KD patients undergoing hematopoietic stem cell transplantation or gene therapy, especially in cases where GALC correction within oligodendrocytes remains deficient or attenuated. One possible extrapolation of this work is that individuals with mutational heterozygosity, single nucleotide polymorphisms, and epigenetic dysregulation of the *GALC* gene may develop adult dysfunctional expression of *GALC* and thus, increase their vulnerability to different adult-onset neurodegenerative disorders, such as MS as well as Parkinson disease, Alzheimer disease, and other adult-onset conditions, which have been linked to lysosomal deficiencies. Likewise, similar synergic interactions may occur with other lysosomal enzymes (e.g., arylsulfatase A, multiple sulfatase). Understanding how these interactions occur will be important to developing improved therapies to treat adult-onset demyelination and neurodegeneration.

MATERIALS AND METHODS

Animals

Animal work in this study was performed in accordance with approved protocols from the Animal Care and Use Committee at the University of Illinois at Chicago. Mice were maintained in a 12-h light/dark cycle at 25°C and received *ad libitum* food and water. Mice genotypes were maintained in a C57BL/6J background. The *Galc-flox* mouse line[31] was kindly donated by Dr. Laura Feltri (State University of New York at Buffalo) and crossed with the *PLP-CRE^{ERT}* mouse line.[32] Resulting *PLP-CRE^{ERT}-Galc-flox* genotypes were confirmed in newborn pups by PCR using specific primers for *Galc-Flox*: P1: 5′-CATCATCCTGTTTCCACAGG, P2: 5′-AATATGTAGGGAGAGAGTGGTC, P3: 5′-CTATTTTAA GG GAGTTCTGCCAGTG and for *PLP-CRE*: F: AGGTGGACCTGAT CATGGAG, R: ATACCG GAGATCATGCAAGC. Non-recombined *Galc*-flox band size is 393 bp; recombined *Galc*-flx is 514 bp and wild type is 266 bp.[31,32] CRE-^{ERT} recombination was done by 5 consecutive daily intraperitoneal injections with 75 mg/kg TMX (Sigma-Aldrich #T5648) starting at P40. Controls received equal daily injections of corn oil. At collection time, mice were anesthetized with isoflurane and transcardially perfused with PBS. Brains were removed and further processed for either biochemistry or histology as outlined below.

EAE induction

EAE was induced by immunization with $MOG_{35–55}$ using the Hooke Kit $MOG_{35–55}$ Emulsion PTX antigen (Cat. N° EK-2110, Hooke Laboratories), according to the manufacturer's instructions. In our experimental design, EAE was initiated on P400 mice. On day 1, mice received two subcutaneous 0.1 mL injections of $MOG_{35–55}$ in complete Freund's adjuvant (CFA), followed by an intraperitoneal administration of 80 ng of pertussis toxin (PTX) diluted in PBS after 2 h. A second equal dose of PTX was given on day 2. Control groups were treated with a mineral oil control for MOG, and PBS control for PTX. Progression of EAE was monitored every other day for the first week and then daily.

Clinical and survival follow-up

The progression of clinical signs was assessed employing a modified version of the DSS system previously established in our lab.[18] DSS exhibits a minimum score of 0 for no observable signs and values of greater than 5 for the most severe clinical signs, which include weight loss, locomotion skill loss, wire hanging latency, hindlimb clasping, and ledge balance (for detailed DSS components, please refer to Marshall et al.[18]). Mice were evaluated weekly by an operator blinded to the genotypes and treatments. In accordance with the Animal Care and Use Committee at the University of Illinois at Chicago, humane end point criteria were considered when mice displayed complete limbs paralysis for 2 consecutive days or exhibited more than 2.0 g of weight loss in two consecutive grading periods. This time point was recorded as the maximal survival point.

A dedicated scoring system was used for EAE experiments as follows: score 0, no obvious changes in motor function compared with control mice; score 1, limp tail; when picked up by the tail, the tail is not erect and drapes over finger; score 2, limp tail and weakness of the hind legs; when picked up by the tail, the legs are not spread apart but held closer together, and mice have wobbly/ataxic gait; score 3, limp tail and complete paralysis of hind legs or urinary incontinence or limp tail with paralysis of one front and one hind leg or severe head tilting, walking along the edges of the cage, pushing against the cage wall, and spinning when picked up by the tail; score 4, limp tail, complete hind leg paralysis, front leg paresis, partial front leg paralysis, or atonic bladder; mouse is minimally moving around the cage but appears alert and is eating and drinking; and score 5, complete hind and front leg paralysis, no movement around the cage. In complement to these analyses, final EAE scoring also considered body weight loss (0 points: no weight loss; 0.5 points, 0–0.5 g weight loss; 1.0 point, 0.6–1.0 g weight loss; 1.5 points, 1.1–2 g weight loss; 2.0 points, >2.0 g weight loss). Upon EAE induction, experimental (and control) animals were scored every other day using this scoring system, until a value of 2 was reached, after which the measurements were performed daily. A score of 3 is needed to increase the measurements to twice per day.

Rotarod test

Training on the rotarod apparatus (San Diego Instruments) was performed over 3 consecutive days, each day at 4 rpm for 5 min × three sets with breaks between each run. Performance was then evaluated once a month in mice between P120 and P240 and then at P400. The rod rotated at 10 rpm for a 5-min maximum period and latency to fall was recorded over three trials with breaks between each run. Latencies to fall in the rotarod below normal values were measured as previously described.[18]

Tissue processing

Collected brains were homogenized in H_2O containing Halt Protease and Phosphatase Inhibitor Cocktail (Thermo Fisher Scientific) by sonication on ice with three pulses of 5 s each at 40% amplitude. Protein concentration of brain homogenates was subsequently measured by the Pierce BCA Protein assay kit (#23225, Thermo Fisher Scientific), using BSA as a reference for the standard curve. Brain lysates were used for analyses of GALC activity, psychosine levels, acid ceramidase (ACD) activity (3 animals were employed for the no TMX and +TMX groups, 8 for EAE group and 10 for TMX+EAE group), or diluted in 2× RIPA buffer for western blotting, respectively (3 animals were used for the no TMX and +TMX groups, and 6 for EAE and TMX+EAE groups).

GALC enzymatic activity

A 30-μL reaction was prepared by mixing 10 μL of equal amounts of protein (30 μg) from brain lysates with 20 μL of the reaction buffer (0.2 M Na_2HPO_4, 0.1 M citric acid buffer, pH 5.2, and 0.02% Na-Azide) containing the fluorescent GALC substrate (6HMU-beta-D-galactoside; moscerdam substrates). Reaction was incubated at 37°C for 17h and stopped by the addition of 200 μL of stop buffer (0.2M glycine/NaOH buffer pH 10.7 + 0.2% Na-SDS + 0.2% Triton X-100). Fluorescence was measured to assess enzyme activity using a Beckmann Coulter DTX 880 multimode detector through excitation/emission wavelengths of 370 nm and 535 nm, respectively. As a blank and negative control for GALC reaction, a similar reaction was performed with 10 μL of 0.2% BSA.

ACD enzymatic activity

Assays were performed according to the protocol previously described.[82] Brain lysates (15 μg) were diluted in a 0.2M sucrose solution to a final volume of 25 μL and mixed with 74.5 μL of 25 mM sodium acetate buffer (pH 4.5) and 0.5 μL of the fluorogenic substrate Rbm14-12 (4 mM). The reaction was incubated for 3 h at 37°C and subsequently stopped by adding 50 μL methanol and 100 μL of a solution of 2.5 mg/mL $NaIO_4$ dissolved in 100 mM glycine/NaOH buffer (pH 10.6). The mixture was protected from light for 2 h at 37°C, and the released fluorescence was measured in a plate reader using excitation/emission wavelengths of 370 nm and 465 nm, respectively. Reaction blanks included all reaction components except enzyme sources.

Psychosine analysis

Psychosine was extracted from 100–200 μg of brain lysates by adding a methanol-acetic acid mixture (0.5% acetic acid in methanol). After 1 h of rotating incubation at room temperature, samples were centrifuged at 16,000×*g* at 4°C and supernatants collected to

determine psychosine content by liquid chromatography-tandem mass spectrometry, as previously described.[18] Lactosyl-(β)-sphingosine (d18:1) was used as an internal standard.

Preparation of mixed glial primary cultures

Brain cortices were obtained from *PLP-CRE^{ERT}-Galc$^{f//f}$* pups at approximately P4, mechanically dissociated in a sterile mesh with Basal Medium (DMEM with 5 mM HEPES, penicillin/streptomycin, and glutamax), and subsequently passed by a metal cell strainer to remove any tissue clamp. Collected cell suspension was centrifuged at 800×*g* for 5 min, and the pellet was resuspended in basal medium +10% fetal bovine serum (FBS). Cells were then plated either on poly-L-Lysine coated coverslips or on a six-well plate, and the culture medium was replaced with fresh basal medium +10% FBS every 3–4 days. For TMX-induced CRE^{ERT} recombination *in vitro*, 14 day *in vitro* cells were treated with 2 μM TMX (Sigma-Aldrich #T5648) for 24 h or with ethanol as a vehicle. The culture medium was replaced, and cells were maintained for additional 7 days before collection for immunocytochemistry, GALC activity, or psychosine measurements.

Immunofluorescence analysis

For immunocytochemistry, mixed glial primary cultures (mouse glial primary culture (MGPCs) were fixed with 4% PFA-PBS for 30 min at room temperature. PFA was washed out with PBS, and cells were incubated overnight at room temperature with rabbit anti-PLP (1:200, a kind gift from late Dr Robert Skoff, Wayne State University, MI), mouse-GALC (1:50, in-house produced monoclonal IgG[83]), rabbit-Olig2 (1:200, in-house produced) and rabbit anti-GFAP (1:1,000, Millipore) primary antibodies diluted in 0.2% BSA 0.1% Triton X-100 PBS. After three washes with PBS, anti-rabbit or anti-mouse secondary antibodies conjugated to Alexa Fluor 488 or 565 (1:1,000) were incubated for 3 h at room temperature. Coverslips were mounted in VECTASHIELD Antifade Mounting Medium with DAPI (H-1200-10, Vector Laboratories). Images were acquired by confocal microscopy (Leica TCS SPE, Wetzlar, Germany).

For immunohistochemistry, fixed brains were cryoprotected in sucrose and optimal cutting temperature embedded before cryosectioning with a Leica CM3050 cryostat (Leica Biosystems). Floating sections (sagittal 30-μm cryosections) were washed with PBS three times for 10 min each, and incubated with rabbit anti-PLP (1:400, a kind gift from Robert Skoff, Wayne University), mouse anti-GALC (1:50, in-house produced monoclonal IgG), rabbit anti-PDGFR-α (1:200, SC-338, Santa Cruz Biotechnology), rat anti-PDGFR-α (1:50, Apa5, BD Pharmingen), rat anti-MBP (1:300, a kind gift from Anthony Campagnoni, UCLA), rat anti-CD68 (1:800, MCA1957GA, Biorad), mouse anti-GFAP (1:800, MAB360, EMD Millipore), rabbit anti-LAMP2 (1:300, PA1-655 Invitrogen), rat anti-LAMP1 (1:400, sc-19992 Santa Cruz Biotechnology), anti-TFEB (1:200, 4240S, Cell Signaling), rabbit anti-Sox10 (1:400, ab 155279, Abcam), rabbit anti-NG2 (1:300, AB5320, EMD Millipore), rabbit anti-SQSTM1/p62 (1:400, D6M5X, Cell Signaling), mouse anti-PCNA (1:400, PC10, Cell Signaling), mouse anti-GFAP (1:600, MAB360, EMD Millipore), mouse anti-APC (1:200, mAb CC-1, Millipore), rabbit anti-cleaved caspase-3 (1:200, AF835, R&D Systems), or rabbit anti-Iba1 (1:200, Fujifilm) primary antibodies diluted in 0.2% BSA 0.1% Triton X-100 PBS. Tissue stained with anti-PCNA, anti-SOX10, and anti-TFEB was pretreated with 0.2N HCl for 20 min at 37°C for antigen retrieval before primary antibody incubation. After three washes with PBS, sections were incubated with the appropriate secondary antibodies conjugated to Alexa Fluor 488, 565, and 635 (1:1,000) for 2 h. After final washes, sections were mounted with VECTASHIELD Antifade Mounting Medium with DAPI. Different brain regions, including cerebellum, upper cortex, medulla oblongata, and hippocampus were imaged by confocal microscopy Leica TCS SPE using 20×, 40×, or 63× objective lens. In these regions, the extent of demyelination was assessed by acquiring the confocal microscopy images with same parameters among all groups, as well as by the quantification of the number of PLP+ debris per field for each experimental condition. To analyze the abundance of cells double-positive for cleaved-caspase 3 and for either CC1, GFAP, CD68, or NeuN, acquired images were analyzed in the respective fluorescence channel by ImageJ using the Cell Counter plug-in. Three representative images per region/per animal/per condition were analyzed with ImageJ software and performed blinded to each experimental condition and group.

Western blotting

Brain lysates were diluted in an equal volume of 2X RIPA (Radio Immuno Precipitation Assay) buffer with protease and phosphatase inhibitors. For SDS-PAGE, 20 μg of proteins were loaded in NuPAGE 4–12% Bis-Tris protein gels (Invitrogen), and separated at 120V, transferred onto polyvinylidene difluoride membranes (Biorad), blocked for 1 h at room temperature with either 3% BSA or 1% Non-fat milk in TBS-tween (TBS-T), and incubated overnight at 4°C with the following primary antibodies: rabbit anti-phospho-TFEB S211 (1:1,000, S211, Cell Signaling), rabbit anti-TFEB (1:2,000 4240S, Cell Signaling), rabbit anti-phospho-AKT (1:2000, S473,Cell Signaling), mouse anti-AKT (1:3,000, 40D4 Cell Signaling), rabbit anti-LC3A/B (1:1,000, 4108 Cell Signaling), chicken anti-GFAP (1:2,000, AB5541 EMD Millipore), rat anti-CD68 (1:1,000, MCA1957GA, Biorad), rabbit anti-Olig2 (1:500, in-house produced), rabbit anti-LAMP2 (1:2,000, PA1-655, Invitrogen), rat anti-LAMP1 (1:1,000, sc-19992 Santa Cruz Biotechnology), rabbit anti-Beclin-1 (1:1,000, D40C5, Cell signaling), rabbit anti-Sox10 (1:1,000, ab155279, Abcam), rabbit anti-SQSTM1/p62 (1:1,000, D6M5X, Cell Signaling), rabbit anti-cleaved caspase-3 (1:1,000, D175, Cell Signaling), mouse anti-GAPDH (1:5,000, CB1001, EMD Millipore), and mouse anti-tubulin (1:5,000, CP06, EMD Millipore). Membranes were washed three times with TBS-T and incubated with IRDye secondary antibodies (1:10,000 Li-COR) for 1 h at room temperature. After three washes with TBS-T, fluorescence signals were acquired using a LiCOR Odyssey CLx Imager.

TEM

Experimental animals were perfused with 0.1 M phosphate buffer (Electron Microscopy Sciences), and the cervical spinal cords were

subsequently removed and fixed with 2.5% paraformaldehyde/2.5% glutaraldehyde in 0.1 M phosphate buffer (pH 7.4) for 24 h at 4°C. For TEM, tissue was embedded in araldite, ultrathin sections prepared and stained at the Electron Microscopy Core of the University of Illinois at Chicago. TEM images were acquired in a EOL JEM-1400 Flash TEM. The percentage of affected axons was calculated considering the number of axons that showed normal myelination, demyelination or remyelination of the total number of axons per case for each experimental condition. Between 300 and 700 axons per experimental group were quantified.

Statistical analysis

Data and graphs were analyzed using GraphPad Prism software version 8.0 (GraphPad Software Inc.). Outliers contained in sample data were identified by ROUT method, with Q value set to 1% in GraphPad Prism software. Statistical analyses were performed using the Student's t-test of unpaired data, or one-way ANOVA followed by Tukey's *post hoc* test for comparisons involving three variables. A p value of less than 0.05 was considered statistically significant.

DATA AND CODE AVAILABILITY

All data necessary for reproducibility are contained in this manuscript. Any other additional information is available upon request to the corresponding author.

SUPPLEMENTAL INFORMATION

Supplemental information can be found online at https://doi.org/10.1016/j.ymthe.2024.06.035.

ACKNOWLEDGMENTS

The authors are grateful to Dr. Swetha Gowrishankar, Dr. Ruth Muchiri, and Mrs. Anne Rugari for insightful discussions. We are grateful to the late Dr. Laura Feltri for donating the *flox-Galc* transgenic line and celebrate her memory with this study. This study was supported by grants from the National Institutes of Health to E.R.B. (R01 NS065808, R01NS127403) and to G.H. (F30 HD103447) and from the Rosenau Family Research Foundation to E.R.B.

AUTHOR CONTRIBUTIONS

N.S., G.H., and D.Z.: design, execute experiments, data analysis, write manuscript; J.W., N.V., A.K., R.S., S.S., D.S., R.V.B., and M.I.G.: execute experiments, data analysis, edit manuscript; E.R.B., secure funding, design, execute experiments, data analysis, write, edit and manuscript submission.

DECLARATION OF INTERESTS

The authors declare absence of any conflict of interest in the preparation, execution, and decision to publish of this study. All data are available upon request.

REFERENCES

1. Barnes-Velez, J.A., Aksoy Yasar, F.B., and Hu, J. (2023). Myelin lipid metabolism and its role in myelination and myelin maintenance. Innovation (Camb) *4*, 100360. https://doi.org/10.1016/j.xinn.2022.100360.

2. Bichenkov, E., and Ellingson, J.S. (1999). Temporal and quantitative expression of the myelin-associated lipids, ethanolamine plasmalogen, galactocerebroside, and sulfatide, in the differentiating CG-4 glial cell line. Neurochem. Res. *24*, 1549–1556. https://doi.org/10.1023/a:1021104232590.

3. Djuanda, D., He, B., Liu, X., Xu, S., Zhang, Y., Xu, Y., and Zhu, Z. (2021). Comprehensive Analysis of Age-related Changes in Lipid Metabolism and Myelin Sheath Formation in Sciatic Nerves. J. Mol. Neurosci. *71*, 2310–2323. https://doi.org/10.1007/s12031-020-01768-5.

4. Luoma, A.M., Kuo, F., Cakici, O., Crowther, M.N., Denninger, A.R., Avila, R.L., Brites, P., and Kirschner, D.A. (2015). Plasmalogen phospholipids protect internodal myelin from oxidative damage. Free Radic. Biol. Med. *84*, 296–310. https://doi.org/10.1016/j.freeradbiomed.2015.03.012.

5. Marangon, D., Boccazzi, M., Lecca, D., and Fumagalli, M. (2020). Regulation of Oligodendrocyte Functions: Targeting Lipid Metabolism and Extracellular Matrix for Myelin Repair. J. Clin. Med. *9*, 470. https://doi.org/10.3390/jcm9020470.

6. Marian, O.C., Teo, J.D., Lee, J.Y., Song, H., Kwok, J.B., Landin-Romero, R., Halliday, G., and Don, A.S. (2023). Disrupted myelin lipid metabolism differentiates frontotemporal dementia caused by GRN and C9orf72 gene mutations. Acta Neuropathol. Commun. *11*, 52. https://doi.org/10.1186/s40478-023-01544-7.

7. Saher, G., Brügger, B., Lappe-Siefke, C., Möbius, W., Tozawa, R.I., Wehr, M.C., Wieland, F., Ishibashi, S., and Nave, K.A. (2005). High cholesterol level is essential for myelin membrane growth. Nat. Neurosci. *8*, 468–475. https://doi.org/10.1038/nn1426.

8. Saher, G., Quintes, S., and Nave, K.A. (2011). Cholesterol: a novel regulatory role in myelin formation. Neuroscientist *17*, 79–93. https://doi.org/10.1177/1073858410373835.

9. Takahashi, H., Perez-Canamas, A., Ye, H., Han, X., and Strittmatter, S.M. (2023). Lysosomal TMEM106B interacts with galactosylceramidase to regulate myelin lipid metabolism. Preprint at bioRxiv. https://doi.org/10.1101/2023.09.14.557804.

10. Khandker, L., Jeffries, M.A., Chang, Y.J., Mather, M.L., Evangelou, A.V., Bourne, J.N., Tafreshi, A.K., Ornelas, I.M., Bozdagi-Gunal, O., Macklin, W.B., and Wood, T.L. (2022). Cholesterol biosynthesis defines oligodendrocyte precursor heterogeneity between brain and spinal cord. Cell Rep. *38*, 110423. https://doi.org/10.1016/j.celrep.2022.110423.

11. Mathews, E.S., and Appel, B. (2016). Cholesterol Biosynthesis Supports Myelin Gene Expression and Axon Ensheathment through Modulation of P13K/Akt/mTor Signaling. J. Neurosci. *36*, 7628–7639. https://doi.org/10.1523/JNEUROSCI.0726-16.2016.

12. Kobayashi, T., Shinoda, H., Goto, I., Yamanaka, T., and Suzuki, Y. (1987). Globoid cell leukodystrophy is a generalized galactosylsphingosine (psychosine) storage disease. Biochem. Biophys. Res. Commun. *144*, 41–46. https://doi.org/10.1016/s0006-291x(87)80472-2.

13. Suzuki, K., and Suzuki, Y. (1970). Globoid cell leucodystrophy (Krabbe's disease): deficiency of galactocerebroside β-galactosidase. Proc. Natl. Acad. Sci. USA *66*, 302–309.

14. Bongarzone, E.R., Escolar, M.L., Gray, S.J., Kafri, T., Vite, C.H., and Sands, M.S. (2016). Insights into the Pathogenesis and Treatment of Krabbe Disease. Pediatr. Endocrinol. Rev. *13*, 689–696.

15. White, A.B., Givogri, M.I., Lopez-Rosas, A., Cao, H., van Breemen, R., Thinakaran, G., and Bongarzone, E.R. (2009). Psychosine accumulates in membrane microdomains in the brain of krabbe patients, disrupting the raft architecture. J. Neurosci. *29*, 6068–6077.

16. Reddy, A.S., Kim, J.H., Hawkins-Salsbury, J.A., Macauley, S.L., Tracy, E.T., Vogler, C.A., Han, X., Song, S.K., Wozniak, D.F., Fowler, S.C., et al. (2011). Bone marrow transplantation augments the effect of brain- and spinal cord-directed adeno-associated virus 2/5 gene therapy by altering inflammation in the murine model of globoid-cell leukodystrophy. J. Neurosci. *31*, 9945–9957. https://doi.org/10.1523/JNEUROSCI.1802-11.2011.

17. Rafi, M.A., Rao, H.Z., Luzi, P., Luddi, A., Curtis, M.T., and Wenger, D.A. (2015). Intravenous injection of AAVrh10-GALC after the neonatal period in twitcher mice results in significant expression in the central and peripheral nervous systems and improvement of clinical features. Mol. Genet. Metab. *114*, 459–466. https://doi.org/10.1016/j.ymgme.2014.12.300.

18. Marshall, M.S., Issa, Y., Jakubauskas, B., Stoskute, M., Elackattu, V., Marshall, J.N., Bogue, W., Nguyen, D., Hauck, Z., Rue, E., et al. (2018). Long-Term Improvement of Neurological Signs and Metabolic Dysfunction in a Mouse Model of Krabbe's Disease after Global Gene Therapy. Mol. Ther. *26*, 874–889. https://doi.org/10.1016/j.ymthe.2018.01.009.

19. Bradbury, A.M., Rafi, M.A., Bagel, J.H., Brisson, B.K., Marshall, M.S., Pesayco Salvador, J., Jiang, X., Swain, G.P., Prociuk, M.L., ODonnell, P.A., et al. (2018). AAVrh10 Gene Therapy Ameliorates Central and Peripheral Nervous System Disease in Canine Globoid Cell Leukodystrophy (Krabbe Disease). Hum. Gene Ther. *29*, 785–801. https://doi.org/10.1089/hum.2017.151.

20. Karumuthil-Melethil, S., Marshall, M.S., Heindel, C., Jakubauskas, B., Bongarzone, E.R., and Gray, S.J. (2016). Intrathecal administration of AAV/GALC vectors in 10-11-day-old twitcher mice improves survival and is enhanced by bone marrow transplant. J. Neurosci. Res. *94*, 1138–1151. https://doi.org/10.1002/jnr.23882.

21. Heller, G.J., Marshall, M.S., Issa, Y., Marshall, J.N., Nguyen, D., Rue, E., Pathmasiri, K.C., Domowicz, M.S., van Breemen, R.B., Tai, L.M., et al. (2021). Waning efficacy in a long-term AAV-mediated gene therapy study in the murine model of Krabbe disease. Mol. Ther. *29*, 1883–1902. https://doi.org/10.1016/j.ymthe.2021.01.026.

22. Scott-Hewitt, N.J., Folts, C.J., Hogestyn, J.M., Piester, G., Mayer-Pröschel, M., and Noble, M.D. (2017). Heterozygote galactocerebrosidase (GALC) mutants have reduced remyelination and impaired myelin debris clearance following demyelinating injury. Hum. Mol. Genet. *26*, 2825–2837. https://doi.org/10.1093/hmg/ddx153.

23. Duchen, L.W., Eicher, E.M., Jacobs, J.M., Scaravilli, F., and Teixeira, F. (1980). Hereditary leucodystrophy in the mouse: the new mutant twitcher. Brain *103*, 695–710.

24. Takahashi, H., and Suzuki, K. (1984). Demyelination in the spinal cord of murine globoid cell leukodystrophy (the twitcher mouse). Acta Neuropathol. *62*, 298–308. https://doi.org/10.1007/BF00687612.

25. Ida, H., Kawame, F., Kim, S.U., and Eto, Y. (1990). Abnormality in cultured oligodendrocytes and Schwann cells isolated from the twitcher mouse. Mol. Chem. Neuropathol. *13*, 195–204. https://doi.org/10.1007/BF03159922.

26. Suzuki, K., and Suzuki, K. (1990). Myelin pathology in the twitcher mouse. Ann. N. Y. Acad. Sci. *605*, 313–324. https://doi.org/10.1111/j.1749-6632.1990.tb42405.x.

27. LeVine, S.M., and Torres, M.V. (1992). Morphological features of degenerating oligodendrocytes in twitcher mice. Brain Res. *587*, 348–352. https://doi.org/10.1016/0006-8993(92)91018-a.

28. Zaka, M., and Wenger, D.A. (2004). Psychosine-induced apoptosis in a mouse oligodendrocyte progenitor cell line is mediated by caspase activation. Neurosci. Lett. *358*, 205–209. https://doi.org/10.1016/j.neulet.2003.12.126.

29. Meng, X.L., Shen, J.S., Watabe, K., Ohashi, T., and Eto, Y. (2005). GALC transduction leads to morphological improvement of the twitcher oligodendrocytes *in vivo*. Mol. Genet. Metab. *84*, 332–343. https://doi.org/10.1016/j.ymgme.2004.12.007.

30. Weinstock, N.I., Shin, D., Dhimal, N., Hong, X., Irons, E.E., Silvestri, N.J., Reed, C.B., Nguyen, D., Sampson, O., Cheng, Y.C., et al. (2020). Macrophages Expressing GALC Improve Peripheral Krabbe Disease by a Mechanism Independent of Cross-Correction. Neuron *107*, 65–81.e9. https://doi.org/10.1016/j.neuron.2020.03.031.

31. Weinstock, N.I., Kreher, C., Favret, J., Nguyen, D., Bongarzone, E.R., Wrabetz, L., Feltri, M.L., and Shin, D. (2020). Brainstem development requires galactosylceramidase and is critical for pathogenesis in a model of Krabbe disease. Nat. Commun. *11*, 5356. https://doi.org/10.1038/s41467-020-19179-w.

32. Doerflinger, N.H., Macklin, W.B., and Popko, B. (2003). Inducible site-specific recombination in myelinating cells. Genesis *35*, 63–72. https://doi.org/10.1002/gene.10154.

33. Devaux, B., Enderlin, F., Wallner, B., and Smilek, D.E. (1997). Induction of EAE in mice with recombinant human MOG, and treatment of EAE with a MOG peptide. J. Neuroimmunol. *75*, 169–173. https://doi.org/10.1016/s0165-5728(97)00019-2.

34. Reynolds, R., Cenci di Bello, I., Dawson, M., and Levine, J. (2001). The response of adult oligodendrocyte progenitors to demyelination in EAE. Prog. Brain Res. *132*, 165–174. https://doi.org/10.1016/s0079-6123(01)32073-3.

35. Zeiss, C.J. (2021). Comparative Milestones in Rodent and Human Postnatal Central Nervous System Development. Toxicol. Pathol. *49*, 1368–1373. https://doi.org/10.1177/01926233211046933.

36. Li, Y., Xu, Y., Benitez, B.A., Nagree, M.S., Dearborn, J.T., Jiang, X., Guzman, M.A., Woloszynek, J.C., Giaramita, A., Yip, B.K., et al. (2019). Genetic ablation of acid ceramidase in Krabbe disease confirms the psychosine hypothesis and identifies a new therapeutic target. Proc. Natl. Acad. Sci. USA *116*, 20097–20103. https://doi.org/10.1073/pnas.1912108116.

37. Rodriguez, M., Prayoonwiwat, N., Howe, C., and Sanborn, K. (1994). Proteolipid protein gene expression in demyelination and remyelination of the central nervous system: a model for multiple sclerosis. J. Neuropathol. Exp. Neurol. *53*, 136–143. https://doi.org/10.1097/00005072-199403000-00004.

38. Chen, Y., Tian, Y., Tian, H., Huang, Q., Fang, Y., Wang, W., Wan, Y., Pan, D., and Xie, M. (2019). Tamoxifen promotes white matter recovery and cognitive functions in male mice after chronic hypoperfusion. Neurochem. Int. *131*, 104566. https://doi.org/10.1016/j.neuint.2019.104566.

39. Pukos, N., and McTigue, D.M. (2020). Delayed short-term tamoxifen treatment does not promote remyelination or neuron sparing after spinal cord injury. PLoS One *15*, e0235232. https://doi.org/10.1371/journal.pone.0235232.

40. Zhang, Z., Park, J.W., Ahn, I.S., Diamante, G., Sivakumar, N., Arneson, D., Yang, X., van Veen, J.E., and Correa, S.M. (2021). Estrogen receptor alpha in the brain mediates tamoxifen-induced changes in physiology in mice. Elife *10*, e63333. https://doi.org/10.7554/eLife.63333.

41. Chistiakov, D.A., Killingsworth, M.C., Myasoedova, V.A., Orekhov, A.N., and Bobryshev, Y.V. (2017). CD68/macrosialin: not just a histochemical marker. Lab. Invest. *97*, 4–13. https://doi.org/10.1038/labinvest.2016.116.

42. Del Grosso, A., Angella, L., Tonazzini, I., Moscardini, A., Giordano, N., Caleo, M., Rocchiccioli, S., and Cecchini, M. (2019). Dysregulated autophagy as a new aspect of the molecular pathogenesis of Krabbe disease. Neurobiol. Dis. *129*, 195–207. https://doi.org/10.1016/j.nbd.2019.05.011.

43. Lim, S.M., Choi, B.O., Oh, S.I., Choi, W.J., Oh, K.W., Nahm, M., Xue, Y., Choi, J.H., Choi, J.Y., Kim, Y.E., et al. (2016). Patient fibroblasts-derived induced neurons demonstrate autonomous neuronal defects in adult-onset Krabbe disease. Oncotarget *7*, 74496–74509. https://doi.org/10.18632/oncotarget.12812.

44. Zigdon, H., Meshcheriakova, A., Farfel-Becker, T., Volpert, G., Sabanay, H., and Futerman, A.H. (2017). Altered lysosome distribution is an early neuropathological event in neurological forms of Gaucher disease. FEBS Lett. *591*, 774–783. https://doi.org/10.1002/1873-3468.12591.

45. Napolitano, G., Esposito, A., Choi, H., Matarese, M., Benedetti, V., Di Malta, C., Monfregola, J., Medina, D.L., Lippincott-Schwartz, J., and Ballabio, A. (2018). mTOR-dependent phosphorylation controls TFEB nuclear export. Nat. Commun. *9*, 3312. https://doi.org/10.1038/s41467-018-05862-6.

46. Parenti, G., Medina, D.L., and Ballabio, A. (2021). The rapidly evolving view of lysosomal storage diseases. EMBO Mol. Med. *13*, e12836. https://doi.org/10.15252/emmm.202012836.

47. Meireles, A.M., Shen, K., Zoupi, L., Iyer, H., Bouchard, E.L., Williams, A., and Talbot, W.S. (2018). The Lysosomal Transcription Factor TFEB Represses Myelination Downstream of the Rag-Ragulator Complex. Dev. Cell *47*, 319–330.e5. https://doi.org/10.1016/j.devcel.2018.10.003.

48. Santambrogio, S., Ricca, A., Maderna, C., Ieraci, A., Aureli, M., Sonnino, S., Kulik, W., Aimar, P., Bonfanti, L., Martino, S., and Gritti, A. (2012). The galactocerebrosidase enzyme contributes to maintain a functional neurogenic niche during early post-natal CNS development. Hum. Mol. Genet. *21*, 4732–4750. https://doi.org/10.1093/hmg/dds313.

49. Iacono, D., Koga, S., Peng, H., Manavalan, A., Daiker, J., Castanedes-Casey, M., Martin, N.B., Herdt, A.R., Gelb, M.H., Dickson, D.W., and Lee, C.W. (2022). Galactosylceramidase deficiency and pathological abnormalities in cerebral white matter of Krabbe disease. Neurobiol. Dis. *174*, 105862. https://doi.org/10.1016/j.nbd.2022.105862.

50. Coetzee, T., Fujita, N., Dupree, J., Shi, R., Blight, A., Suzuki, K., Suzuki, K., and Popko, B. (1996). Myelination in the absence of galactocerebroside and sulfatide: normal structure with abnormal function and regional instability. Cell *86*, 209–219. https://doi.org/10.1016/s0092-8674(00)80093-8.

51. Kondo, Y., Wenger, D.A., Gallo, V., and Duncan, I.D. (2005). Galactocerebrosidase-deficient oligodendrocytes maintain stable central myelin by exogenous replacement

of the missing enzyme in mice. Proc. Natl. Acad. Sci. USA *102*, 18670–18675. https://doi.org/10.1073/pnas.0506473102.

52. Wenger, D.A., Victoria, T., Rafi, M.A., Luzi, P., Vanier, M.T., Vite, C., Patterson, D.F., and Haskins, M.H. (1999). Globoid cell leukodystrophy in cairn and West Highland white terriers. J. Hered. *90*, 138–142. https://doi.org/10.1093/jhered/90.1.138.

53. Marshall, M.S., Jakubauskas, B., Bogue, W., Stoskute, M., Hauck, Z., Rue, E., Nichols, M., DiAntonio, L.L., van Breemen, R.B., Kordower, J.H., et al. (2018). Analysis of age-related changes in psychosine metabolism in the human brain. PLoS One *13*, e0193438. https://doi.org/10.1371/journal.pone.0193438.

54. Senkevich, K., Zorca, C.E., Dworkind, A., Rudakou, U., Somerville, E., Yu, E., Ermolaev, A., Nikanorova, D., Ahmad, J., Ruskey, J.A., et al. (2023). GALC variants affect galactosylceramidase enzymatic activity and risk of Parkinson's disease. Brain *146*, 1859–1872. https://doi.org/10.1093/brain/awac413.

55. International Multiple Sclerosis Genetics Consortium; Wellcome Trust Case Control Consortium 2, Sawcer, S., Hellenthal, G., Pirinen, M., Spencer, C.C.A., Patsopoulos, N.A., Moutsianas, L., Dilthey, A., Su, Z., et al. (2011). Genetic risk and a primary role for cell-mediated immune mechanisms in multiple sclerosis. Nature *476*, 214–219. https://doi.org/10.1038/nature10251.

56. Sahai, I., Baris, H., Kimonis, V., and Levy, H.L. (2005). Krabbe disease: severe neonatal presentation with a family history of multiple sclerosis. J. Child Neurol. *20*, 826–828. https://doi.org/10.1177/08830738050200100901.

57. Li, H., Hou, X., Liang, Y., Xu, F., Zhang, X., Cui, P., Xing, G., Wang, X., and Jiang, W. (2021). Gene-Based Tests of a Genome-Wide Association Study Dataset Highlight Novel Multiple Sclerosis Risk Genes. Front. Neurosci. *15*, 614528. https://doi.org/10.3389/fnins.2021.614528.

58. Scaravilli, F., and Suzuki, K. (1983). Enzyme replacement in grafted nerve of twitcher mouse. Nature *305*, 713–715. https://doi.org/10.1038/305713a0.

59. Kaminski, D., Yaghootfam, C., Matthes, F., Reßing, A., Gieselmann, V., and Matzner, U. (2021). Brain cell type-specific endocytosis of arylsulfatase A identifies limitations of enzyme-based therapies for metachromatic leukodystrophy. Hum. Mol. Genet. *29*, 3807–3817. https://doi.org/10.1093/hmg/ddaa277.

60. Mikulka, C.R., Dearborn, J.T., Benitez, B.A., Strickland, A., Liu, L., Milbrandt, J., and Sands, M.S. (2020). Cell-autonomous expression of the acid hydrolase galactocerebrosidase. Proc. Natl. Acad. Sci. USA *117*, 9032–9041. https://doi.org/10.1073/pnas.1917675117.

61. Lampron, A., Larochelle, A., Laflamme, N., Préfontaine, P., Plante, M.M., Sánchez, M.G., Yong, V.W., Stys, P.K., Tremblay, M.È., and Rivest, S. (2015). Inefficient clearance of myelin debris by microglia impairs remyelinating processes. J. Exp. Med. *212*, 481–495. https://doi.org/10.1084/jem.20141656.

62. Franklin, R.J.M., and Gallo, V. (2014). The translational biology of remyelination: past, present, and future. Glia *62*, 1905–1915. https://doi.org/10.1002/glia.22622.

63. Gensert, J.M., and Goldman, J.E. (1997). Endogenous progenitors remyelinate demyelinated axons in the adult CNS. Neuron *19*, 197–203. https://doi.org/10.1016/s0896-6273(00)80359-1.

64. D'Auria, L., Reiter, C., Ward, E., Moyano, A.L., Marshall, M.S., Nguyen, D., Scesa, G., Hauck, Z., van Breemen, R., Givogri, M.I., and Bongarzone, E.R. (2017). Psychosine enhances the shedding of membrane microvesicles: Implications in demyelination in Krabbe's disease. PLoS One *12*, e0178103. https://doi.org/10.1371/journal.pone.0178103.

65. Cantuti-Castelvetri, L., Fitzner, D., Bosch-Queralt, M., Weil, M.T., Su, M., Sen, P., Ruhwedel, T., Mitkovski, M., Trendelenburg, G., Lütjohann, D., et al. (2018). Defective cholesterol clearance limits remyelination in the aged central nervous system. Science *359*, 684–688. https://doi.org/10.1126/science.aan4183.

66. Cunha, M.I., Su, M., Cantuti-Castelvetri, L., Müller, S.A., Schifferer, M., Djannatian, M., Alexopoulos, I., van der Meer, F., Winkler, A., van Ham, T.J., et al. (2020). Pro-inflammatory activation following demyelination is required for myelin clearance and oligodendrogenesis. J. Exp. Med. *217*, e20191390. https://doi.org/10.1084/jem.20191390.

67. Hickman, S.E., Allison, E.K., and El Khoury, J. (2008). Microglial dysfunction and defective beta-amyloid clearance pathways in aging Alzheimer's disease mice. J. Neurosci. *28*, 8354–8360. https://doi.org/10.1523/JNEUROSCI.0616-08.2008.

68. Mawuenyega, K.G., Sigurdson, W., Ovod, V., Munsell, L., Kasten, T., Morris, J.C., Yarasheski, K.E., and Bateman, R.J. (2010). Decreased clearance of CNS beta-amyloid in Alzheimer's disease. Science *330*, 1774. https://doi.org/10.1126/science.1197623.

69. Ferguson, B., Matyszak, M.K., Esiri, M.M., and Perry, V.H. (1997). Axonal damage in acute multiple sclerosis lesions. Brain *120*, 393–399. https://doi.org/10.1093/brain/120.3.393.

70. Lovas, G., Szilágyi, N., Majtényi, K., Palkovits, M., and Komoly, S. (2000). Axonal changes in chronic demyelinated cervical spinal cord plaques. Brain *123*, 308–317. https://doi.org/10.1093/brain/123.2.308.

71. Podbielska, M., Banik, N.L., Kurowska, E., and Hogan, E.L. (2013). Myelin recovery in multiple sclerosis: the challenge of remyelination. Brain Sci. *3*, 1282–1324. https://doi.org/10.3390/brainsci3031282.

72. Franco-Juarez, B., Coronel-Cruz, C., Hernandez-Ochoa, B., Gomez-Manzo, S., Cardenas-Rodriguez, N., Arreguin-Espinosa, R., Bandala, C., Canseco-Avila, L.M., and Ortega-Cuellar, D. (2022). TFEB; Beyond Its Role as an Autophagy and Lysosomes Regulator. Cells *11*, 3153. https://doi.org/10.3390/cells11193153.

73. Tanaka, Y., Guhde, G., Suter, A., Eskelinen, E.L., Hartmann, D., Lüllmann-Rauch, R., Janssen, P.M., Blanz, J., von Figura, K., and Saftig, P. (2000). Accumulation of autophagic vacuoles and cardiomyopathy in LAMP-2-deficient mice. Nature *406*, 902–906. https://doi.org/10.1038/35022595.

74. Eskelinen, E.L., Illert, A.L., Tanaka, Y., Schwarzmann, G., Blanz, J., Von Figura, K., and Saftig, P. (2002). Role of LAMP-2 in lysosome biogenesis and autophagy. Mol. Biol. Cell *13*, 3355–3368. https://doi.org/10.1091/mbc.e02-02-0114.

75. Micsenyi, M.C., Sikora, J., Stephney, G., Dobrenis, K., and Walkley, S.U. (2013). Lysosomal membrane permeability stimulates protein aggregate formation in neurons of a lysosomal disease. J. Neurosci. *33*, 10815–10827. https://doi.org/10.1523/JNEUROSCI.0987-13.2013.

76. Sun, Y., Liou, B., Ran, H., Skelton, M.R., Williams, M.T., Vorhees, C.V., Kitatani, K., Hannun, Y.A., Witte, D.P., Xu, Y.H., and Grabowski, G.A. (2010). Neuronopathic Gaucher disease in the mouse: viable combined selective saposin C deficiency and mutant glucocerebrosidase (V394L) mice with glucosylsphingosine and glucosylceramide accumulation and progressive neurological deficits. Hum. Mol. Genet. *19*, 1088–1097. https://doi.org/10.1093/hmg/ddp580.

77. Chevrier, M., Brakch, N., Celine, L., Genty, D., Ramdani, Y., Moll, S., Djavaheri-Mergny, M., Brasse-Lagnel, C., Annie Laquerriere, A.L., Barbey, F., and Bekri, S. (2010). Autophagosome maturation is impaired in Fabry disease. Autophagy *6*, 589–599. https://doi.org/10.4161/auto.6.5.11943.

78. Vergarajauregui, S., Connelly, P.S., Daniels, M.P., and Puertollano, R. (2008). Autophagic dysfunction in mucolipidosis type IV patients. Hum. Mol. Genet. *17*, 2723–2737. https://doi.org/10.1093/hmg/ddn174.

79. Boyao, Y., Mengjiao, S., Caicai, B., Xiaoling, L., Zhenxing, L., and Manxia, W. (2019). Dynamic expression of autophagy-related factors in autoimmune encephalomyelitis and exploration of curcumin therapy. J. Neuroimmunol. *337*, 577067. https://doi.org/10.1016/j.jneuroim.2019.577067.

80. Igci, M., Baysan, M., Yigiter, R., Ulasli, M., Geyik, S., Bayraktar, R., Bozgeyik, İ., Bozgeyik, E., Bayram, A., and Cakmak, E.A. (2016). Gene expression profiles of autophagy-related genes in multiple sclerosis. Gene *588*, 38–46. https://doi.org/10.1016/j.gene.2016.04.042.

81. Sural-Fehr, T., Singh, H., Cantuti-Catelvetri, L., Zhu, H., Marshall, M.S., Rebiai, R., Jastrzebski, M.J., Givogri, M.I., Rasenick, M.M., and Bongarzone, E.R. (2019). Inhibition of the IGF-1-PI3K-Akt-mTORC2 pathway in lipid rafts increases neuronal vulnerability in a genetic lysosomal glycosphingolipidosis. Dis. Model. Mech. *12*, dmm036590. https://doi.org/10.1242/dmm.036590.

82. Bedia, C., Camacho, L., Abad, J.L., Fabriàs, G., and Levade, T. (2010). A simple fluorogenic method for determination of acid ceramidase activity and diagnosis of Farber disease. J. Lipid Res. *51*, 3542–3547. https://doi.org/10.1194/jlr.D010033.

83. Rebiai, R., Rue, E., Zaldua, S., Nguyen, D., Scesa, G., Jastrzebski, M., Foster, R., Wang, B., Jiang, X., Tai, L., et al. (2022). CRISPR-Cas9 Knock-In of T513M and G41S Mutations in the Murine beta-Galactosyl-Ceramidase Gene Re-capitulates Early-Onset and Adult-Onset Forms of Krabbe Disease. Front. Mol. Neurosci. *15*, 896314. https://doi.org/10.3389/fnmol.2022.896314.